Key Engineering Materials, Volume 1033, November 2025, pp. 59-70
DOI: 10.4028/p-ebn8qs

Comparison of the time varying mesh stiffness of gears with single and multi-mode damage.

Aselimhe Oreavbiere[1, a], Muhammad Khan[1, b*]
[1]Faculty of Engineering and Applied Sciences, Cranfield University, Cranfield, United Kingdom

[a]aselimhe.oreavbiere@cranfield.ac.uk , [b]Muhammad.A.Khan@cranfield.ac.uk

Keywords: Spur Gears, Pitting, Spalling, Tooth Crack, Mesh Stiffness.

Abstract. Gears in service conditions experience inevitable tooth damage. These damages can cause changes in the time-varying mesh stiffness (TVMS) depending on the mode of damage. The TVMS of gears is an essential input in calculating gear dynamic responses. Several researchers have evaluated the mesh stiffness of gear teeth with single-mode damage like pitting, spalling, root cracks and wear using either or any combination of analytical, numeric and experimental models. However, limited research has been done on investigating the mesh stiffness of gear teeth undergoing multi-mode damage. In this work, an analytical model is proposed to evaluate the mesh stiffness of a tooth on the pinion with single-mode damage, including pitting, spalling, and surface crack, separately. In addition, a gear tooth with a combination of pits, spalling and surface cracks is also evaluated. The volume of damage on the tooth is kept constant to provide a basis for comparison. The comparison highlights the possible effects of the combined damage modes, which is a more realistic occurrence in gears in service.

Introduction

The time-varying mesh stiffness (TVMS) of gears is a major input in evaluating the dynamic response of gears. It is a source of excitation and can be used as a preliminary means to analyze the changes due to fault on the gear surface [1]. Various methods have been used to determine gear mesh stiffness, some of which include analytical, approximated analytical, hybrid and FEM Models[2]. For analytical modelling, the potential energy method has been widely researched and has been validated with FEM[3]. In this method, the sum of the stiffnesses due to the hertzian, axial, bending and shear energies are determined[4,5]. This analytical method has been used to determine the mesh stiffness of gears with single faults like pitting[6–15], spalling [16–27], root crack[28–37], surface crack [38] and wear[39–42]. To provide more realistic mesh stiffness for gear dynamic responses, it is necessary to calculate mesh stiffness for gear tooths with more than one fault. Research on obtaining gear mesh stiffness for a combination of different faults mode is still limited, However, in [43], different severity modes of pitting and crack faults were combined and the TVMS obtained. The interactions between the two damages were analyzed and mathematical formulations provided for different combinations of severity. From case studies on failures of wind turbine gear boxes, gearboxes in manufacturing plants and in automobiles [44–47], pitting was noted to be the most common occurring fault, pitting often progresses to spalling, and cracks initiated from the pits/spalls develop to tooth surface crack. Several industrial cases had partial tooth breakage which were not initiated at the tooth root. As study on the mesh stiffness of gear with multiple faults progresses, it is important to understand how the different single faults and multiple faults affect the mesh stiffness. In this work, the mesh stiffness for multiple faults on a gear tooth surface consisting of pits, spall and surface crack is determined and a direct comparison is done with the mesh stiffness obtained from the single faults of pitting, spall and surface crack. The fault volume is constant in all four cases. The comparison of the TVMS will help ascertain the similarities and critical differences between the single fault curves and the TVMS curve for the multiple faults.

Published by Trans Tech Publications. This is the Author Accepted Manuscript issued with: Creative Commons Attribution License (CC:BY 4.0).
The final published version (version of record) is available online at DOI:10.4028/p-ebn8qs. Please refer to any applicable publisher terms of use.

Evaluation of Mesh Stiffness

As the gear rotates, the contact point on the pinion and driven gear changes continuously. The mesh stiffness at these points is obtained and plotted against the angle of rotation to obtain the TVMS curve. The equations for the mesh stiffness have one changing variable which is the pressure angle at the contact point. The formulations for the pressure angle and the stiffnesses are derived in [5]. They are presented as equations 1 – 2. Depending on the contact ratio of the gears in mesh, there is a region where two tooth pairs are in contact and a region where a single tooth pair are in contact. The duration of these regions has been derived in [5] and are also shown as equations 3 – 4. The following assumptions are made in the evaluation of the mesh stiffness.

1. There are no manufacturing errors on the gear tooth
2. The effect of friction is neglected
3. The effect of lubrication is neglected
4. Pits are assumed to be of circular cross-section
5. Spalls are assumed to be rectangular cross-section
6. Cracks are assumed to propagate along a straight line
7. Crack depth is uniform along the tooth width

$$\alpha_{1p} = \theta_1 - \frac{\pi}{2N_p} - \boldsymbol{inv}\,\alpha_o + \tan\left[\cos^{-1}\frac{N_p\cos\alpha_o}{\sqrt{(N_g+2)^2 + (N_p+N_g)^2 - 2(N_g+2)(N_p+N_g)\cos\left(\cos^{-1}\left(\frac{N_g\cos\alpha_o}{N_g+2}\right) - \alpha_o\right)}}\right] \quad (1)$$

$$\alpha_{1g} = \tan\left[\cos^{-1}\left(\frac{N_g\cos\alpha_o}{N_g+2}\right)\right] - \frac{\pi}{2N_g} - \boldsymbol{inv}\,\alpha_o - \frac{N_p}{N_g}\theta_1 \quad (2)$$

$$\theta_d = \tan\left[\cos^{-1}\left(\frac{N_p\cos\alpha_o}{N_p+2}\right)\right] - \frac{2\pi}{N_p} - \tan\left[\cos^{-1}\frac{N_p\cos\alpha_o}{\sqrt{(N_g+2)^2 + (N_p+N_g)^2 - 2(N_g+2)(N_p+N_g)\cos\left(\cos^{-1}\left(\frac{N_g\cos\alpha_o}{N_g+2}\right) - \alpha_o\right)}}\right] \quad (3)$$

$$\theta_s = \frac{2\pi}{N_p} - \theta_d \quad (4)$$

Where

α_{1p} =Pressure angle at contact point on pinion

α_{1g} =Pressure angle at contact point on gear

N_p = Number of teeth on pinion

N_g = Number of teeth on gear

θ_1 = Angle of rotation of pinion

α_o = pressure angle

θ_d =the angular duration of the double tooth engagement

θ_s =the angular duration of the single tooth engagement

The pressure angle of the contact points for the second pair of engagement contact points is obtained by adding $\frac{2\pi}{N_p}$ and $\frac{2\pi}{N_g}$ to equations 1 and 2 respectively. The equations for the total mesh stiffness for the single and double tooth engagement region can be calculated by using equations 5 – 7 [3]

$$\frac{1}{K_{t_{1,2}}} = \frac{1}{K_{b_p}} + \frac{1}{K_{s_p}} + \frac{1}{K_{a_p}} + \frac{1}{K_{b_g}} + \frac{1}{K_{s_g}} + \frac{1}{K_{a_g}} + \frac{1}{K_h} \tag{5}$$

For the region of single tooth pair engagement

$$K_m = K_{t1} \tag{6}$$

For the region of double tooth pair engagement

$$K_m = K_{t1} + K_{t2} \tag{7}$$

Note that the stiffness subscripts *b, s, a,* and *h* represent bending, shear, axial, and hertzian stiffnesses. In this work, only gears with teeth below 42 are considered, and the fillet foundation stiffness is ignored.

Healthy Gears. The formulations for the hertzian, bending, axial and shear stiffnesses have been derived in [5]. The equations are shown below as equations 8 - 11. Figure 1[3] shows the healthy gear model.

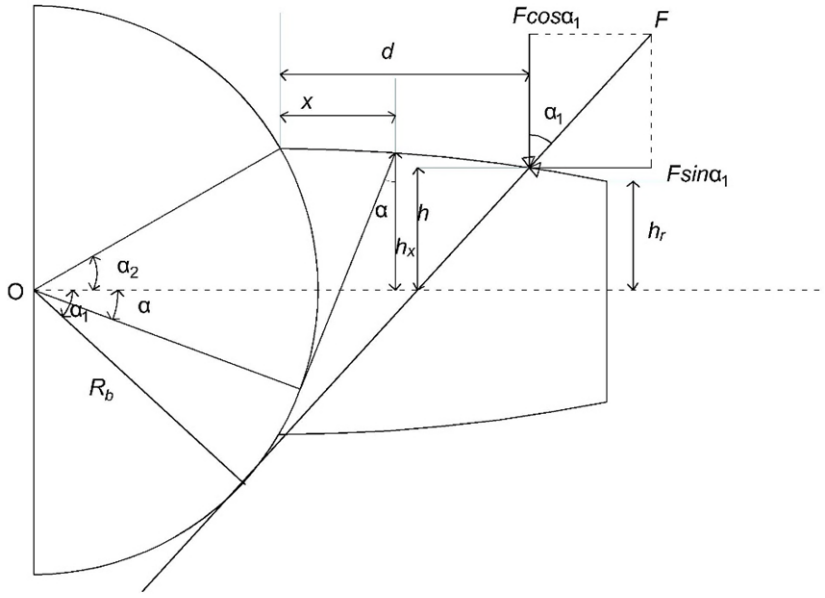

Figure 1: Healthy Gear tooth

$$\frac{1}{K_h} = \frac{4(1-v^2)}{\pi EL} \tag{8}$$

$$\frac{1}{K_a} = \int_{-\alpha_1}^{\alpha_2} \frac{(\alpha_2 - \alpha)\cos\alpha \sin^2\alpha_1}{2EL[\sin\alpha + (\alpha_2 - \alpha)\cos\alpha]} d\alpha \tag{9}$$

$$\frac{1}{K_b} = \int_{-\alpha_1}^{\alpha_2} \frac{3\{1 + \cos\alpha_1[(\alpha_2 - \alpha)\sin\alpha - \cos\alpha]\}^2(\alpha_2 - \alpha)\cos\alpha}{2EL[\sin\alpha + (\alpha_2 - \alpha)\cos\alpha]^3} d\alpha \tag{10}$$

$$\frac{1}{K_s} = \int_{-\alpha_1}^{\alpha_2} \frac{1.2(1+v)(\alpha_2 - \alpha)\cos\alpha\cos^2\alpha}{2EL[\sin\alpha + (\alpha_2 - \alpha)\cos\alpha]} d\alpha \quad (11)$$

Where
v = poison ratio
E = Modulus of Elasticity

Gear tooth with pitting damage. In pitting, the cross-sectional area of the contact point has changes in its tooth width, area, area, area moment of inertia due to the pits. This affects the bending stiffness, shear stiffness, axial stiffness and hertzian contact stiffness. Figure 2 shows a gear tooth with pits and the dimensions of the pits. The length (L), area (A), area moment of inertia due to the pits can be calculated and included in equations 8 to 11. The pits are assumed to be circular in cross-section and evenly distributed. The changes due to pitting on the geometry can be calculated as shown

$$L_p = nl_p \quad (12)$$

$$A_p = nl_p h_p \quad (13)$$

$$I_p = \frac{1}{12} h_p^3 l_p n \quad (14)$$

Where
n = number of pits
l_p = length of chord of circular pit at the cross -section of contact
h_p = depth of pit

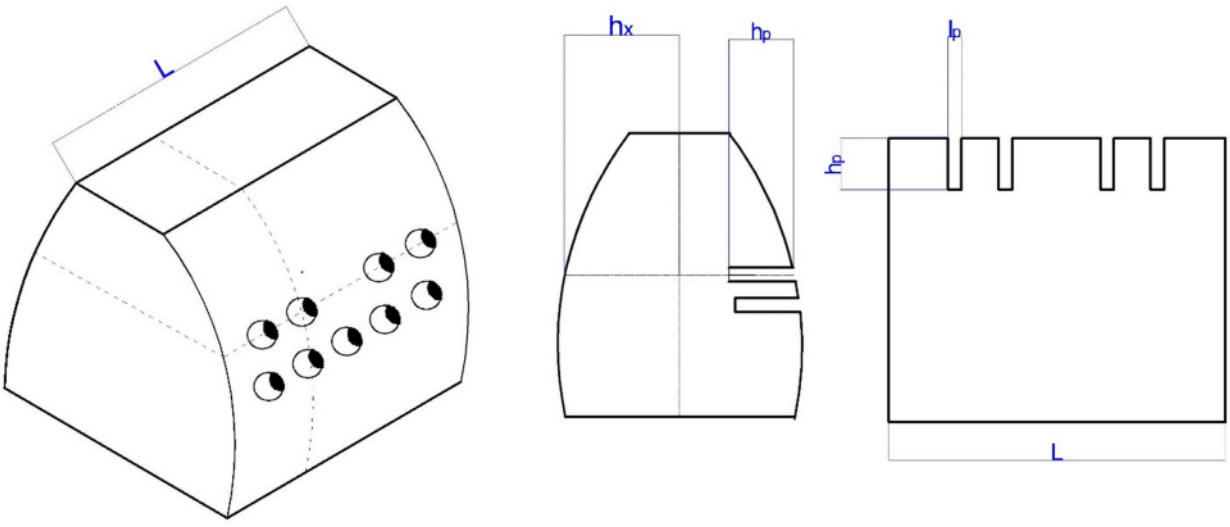

Figure 2: Tooth with Pitting damage

These can be subtracted from the corresponding values of the healthy system to obtain the values due to the pits as shown. The equations for the axial, hertzian and bending stiffnesses for the gear tooth [43] are presented as equations 15 -18

$$\frac{1}{K_h} = \frac{4(1-\nu^2)}{\pi E(L-L_p)} \tag{15}$$

$$\frac{1}{K_a} = \int_{-\alpha_1}^{\alpha_2} \frac{(\alpha_2-\alpha)\cos\alpha\sin^2\alpha_1}{E\left\{\langle 2L[\sin\alpha+(\alpha_2-\alpha)\cos\alpha]\rangle - \frac{A_p}{R_b}\right\}}d\alpha \tag{16}$$

$$\frac{1}{K_b} = \int_{-\alpha_1}^{\alpha_2} \frac{3\{1+\cos\alpha_1[(\alpha_2-\alpha)\sin\alpha-\cos\alpha]\}^2(\alpha_2-\alpha)\cos\alpha}{E\left\{2L[\sin\alpha+(\alpha_2-\alpha)\cos\alpha]^3 - 3\frac{I_p}{R_b{}^3}\right\}}d\alpha \tag{17}$$

$$\frac{1}{K_s} = \int_{-\alpha_1}^{\alpha_2} \frac{1.2(1+v)(\alpha_2-\alpha)\cos\alpha\cos^2\alpha}{E\left\{\langle L[\sin\alpha+(\alpha_2-\alpha)\cos\alpha]\rangle - 0.5\frac{A_p}{R_b}\right\}}d\alpha \tag{18}$$

Gear tooth with spall damage. The spalling damage affects all the stiffnesses like that of pitting. The values of area, moment of inertia and length due to the spall is as shown in figure 3. The spall is assumed to be a rectangular cross-section on the gear surface. The equations due to the spall are shown in equations in equation 19 -21

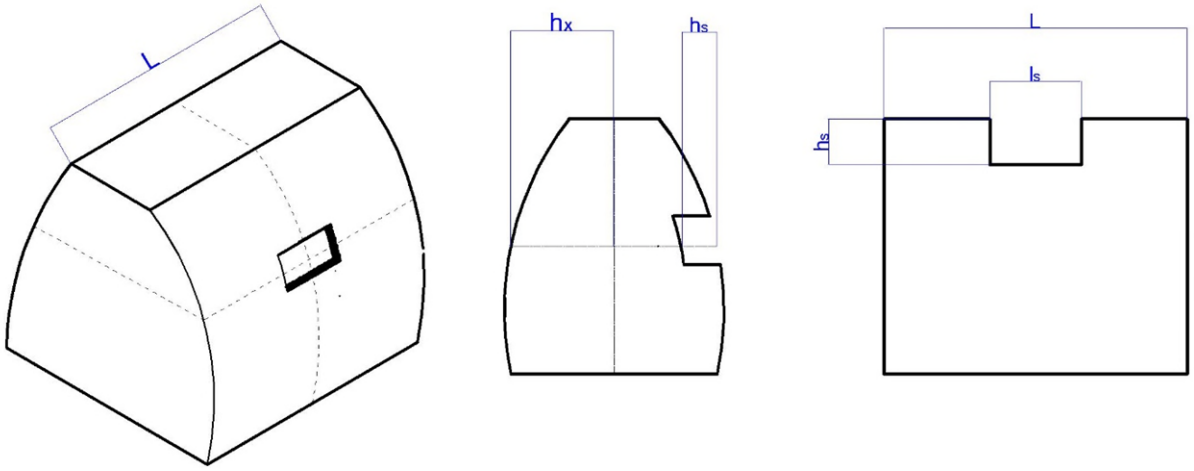

Figure 3: Tooth with spall

$$L_s = l_s \tag{19}$$

$$A_s = l_s h_s \tag{20}$$

$$I_s = \frac{1}{12}h_s^3 l_s \tag{21}$$

The equations for stiffness become

$$\frac{1}{K_h} = \frac{4(1-\nu^2)}{\pi E(L-L_s)} \tag{22}$$

$$\frac{1}{K_a} = \int_{-\alpha_1}^{\alpha_2} \frac{(\alpha_2-\alpha)\cos\alpha\sin^2\alpha_1}{E\left\{\langle 2L[\sin\alpha+(\alpha_2-\alpha)\cos\alpha]\rangle - \frac{A_s}{R_b}\right\}}d\alpha \tag{23}$$

$$\frac{1}{K_b} = \int_{-\alpha_1}^{\alpha_2} \frac{3\{1+\cos\alpha_1[(\alpha_2-\alpha)\sin\alpha-\cos\alpha]\}^2(\alpha_2-\alpha)\cos\alpha}{E\left\{2L[\sin\alpha+(\alpha_2-\alpha)\cos\alpha]^3 - 3\frac{I_s}{R_b{}^3}\right\}}d\alpha \tag{24}$$

$$\frac{1}{K_s} = \int_{-\alpha_1}^{\alpha_2} \frac{1.2(1+v)(\alpha_2-\alpha)\cos\alpha\cos^2\alpha}{E\left\{\langle L[\sin\alpha+(\alpha_2-\alpha)\cos\alpha]\rangle - 0.5\frac{A_s}{R_b}\right\}}d\alpha \tag{25}$$

Gear tooth with surface crack damage. The crack is assumed to be straight and for the full length of the tooth width. The crack fault does not affect the axial and hertzian stiffness of the gear [5]. The formular for the area and moment of inertia due to the crack are shown as equations 26 -27. Figure 4 shows the dimensions used in the formulars.

$$A_c = Lh_{cx} \tag{26}$$

$$I_c = \frac{1}{12}h_{cx}^3 L \tag{27}$$

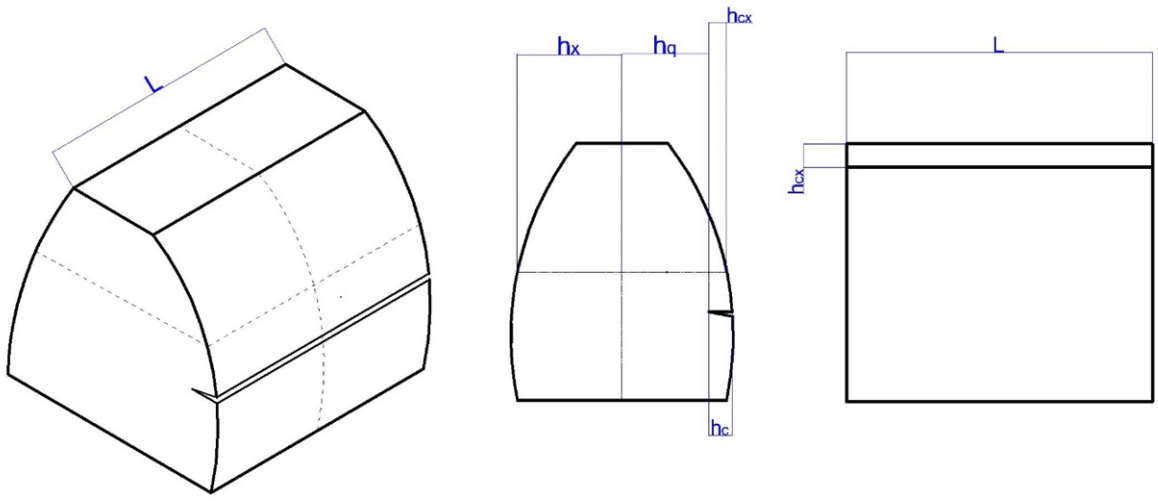

Figure 4: Tooth with surface crack

The bending and shear stiffnesses can be calculated using the formulars in equations 28 -29.

$$\frac{1}{K_b} = \int_{-\alpha_1}^{\alpha_2} \frac{3\{1+\cos\alpha_1[(\alpha_2-\alpha)\sin\alpha-\cos\alpha]\}^2(\alpha_2-\alpha)\cos\alpha}{E\left\{2L[\sin\alpha+(\alpha_2-\alpha)\cos\alpha]^3 - 3\frac{I_c}{R_b{}^3}\right\}}d\alpha \tag{28}$$

$$\frac{1}{K_s} = \int_{-\alpha_1}^{\alpha_2} \frac{1.2(1+v)(\alpha_2-\alpha)\cos\alpha\cos^2\alpha}{E\left\{\langle L[\sin\alpha + (\alpha_2-\alpha)\cos\alpha]\rangle - 0.5\frac{A_c}{R_b}\right\}} d\alpha \quad (29)$$

Gear tooth with pitting, spall and surface crack. In the previous damage tooth discussed, the gear contact points will move between healthy sections and the single fault sections and then healthy sections before disengagement. However, in multiple fault gear tooth, there is a continuous change in the cross sections of the contact points. Figure 5 presents a combination of pitting, spall and surface crack. The contact points for the gear tooth in figure 5 will follow the following sequence from the base

Section 1 – No fault -
Section 2 – Surface crack fault only
Section 3 – Surface crack and pits
Section 4 – Surface crack only
Section 5 – Surface crack and spall
Section 6 – Surface crack, pit and spall
Section 7 – Pit and spall
Section 8 – Spall
Section 9 – No fault

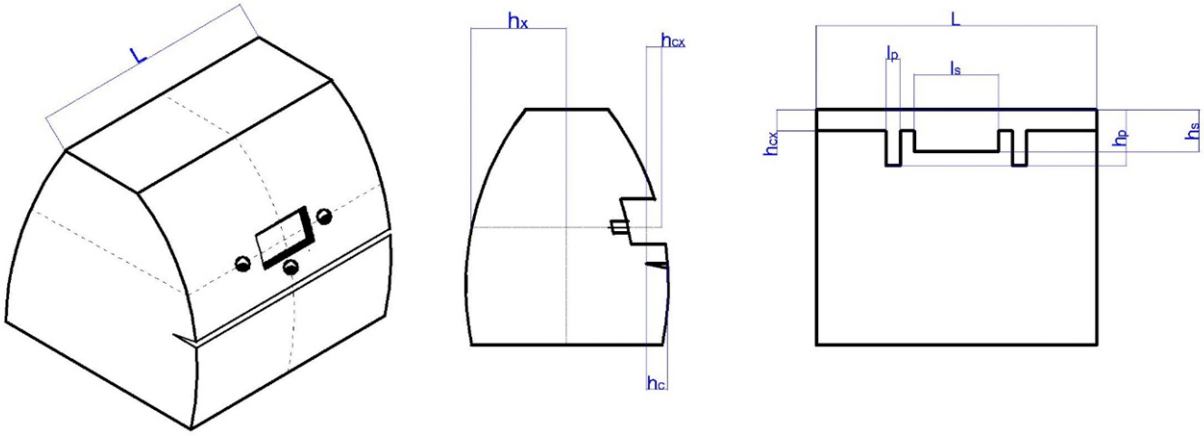

Figure 5: Gear tooth with pitting, spall and surface crack

For the section shown in the diagram, which is a combination of Surface crack, pits and spall. The equations for the length, area and area moment of inertia are shown in equations

$$L_m = nl_p + l_s \quad (30)$$

$$A_m = h_{cx}L + nl_p(h_p - h_{cx}) + l_s(h_s - h_{cx}) \quad (31)$$

$$I_m = \frac{1}{12}\left[h_{cx}{}^3 L + nl_p(h_p - h_{cx})^3 + l_s(h_s - h_{cx})^3\right] \quad (32)$$

Equations 30 – 32 are included in the stiffness equations as shown in equations 33 – 36.

$$\frac{1}{K_h} = \frac{4(1-\nu^2)}{\pi E(L-L_m)} \tag{33}$$

$$\frac{1}{K_a} = \int_{-\alpha_1}^{\alpha_2} \frac{(\alpha_2-\alpha)\cos\alpha\sin^2\alpha_1}{E\left\{\langle 2L[\sin\alpha+(\alpha_2-\alpha)\cos\alpha]\rangle - \frac{A_m}{R_b}\right\}} d\alpha \tag{34}$$

$$\frac{1}{K_b} = \int_{-\alpha_1}^{\alpha_2} \frac{3\{1+\cos\alpha_1[(\alpha_2-\alpha)\sin\alpha-\cos\alpha]\}^2(\alpha_2-\alpha)\cos\alpha}{E\left\{2L[\sin\alpha+(\alpha_2-\alpha)\cos\alpha]^3 - 3\frac{I_m}{R_b{}^3}\right\}} d\alpha \tag{35}$$

$$\frac{1}{K_s} = \int_{-\alpha_1}^{\alpha_2} \frac{1.2(1+\nu)(\alpha_2-\alpha)\cos\alpha\cos^2\alpha}{E\left\{\langle L[\sin\alpha+(\alpha_2-\alpha)\cos\alpha]\rangle - 0.5\frac{A_m}{R_b}\right\}} d\alpha \tag{36}$$

Comparison of the TVMS

The TVMS for a gear pair with details shown in table 1 was simulated with MATLAB to obtain the TVMS curves for the healthy, single fault gear tooth and gear tooth with multiple faults. The TVMS curves are presented as figure 6 and 7

Table 1: Gear details

	Pinion	Wheel
Outer Diameter(mm)	130	135
Module	5	
No of Teeth	24	25
Pressure angle	20	

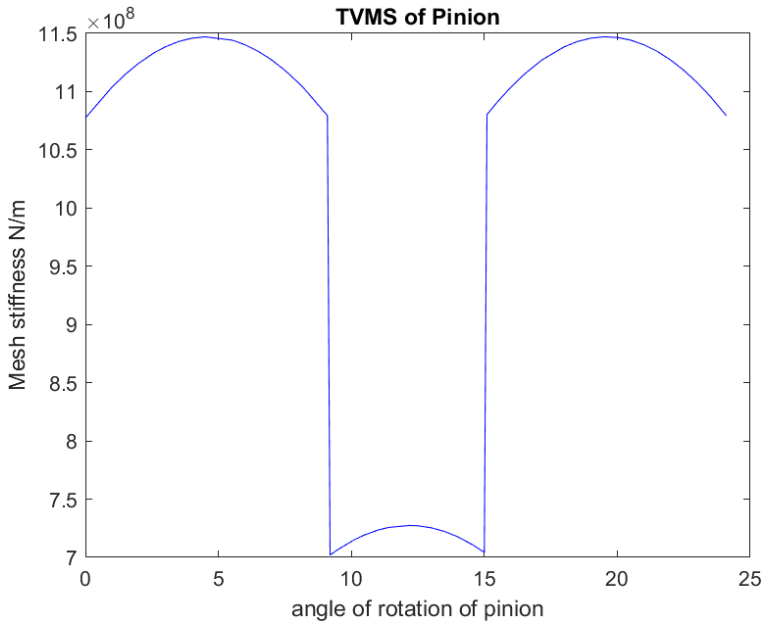

Figure 6: TVMS of Healthy Gear Pair

0.96% of the pinion's volume was the fixed volume of all the faults and this resulted in the following dimension of faults

1. 9 pits of radius 0.7±0.1mm and depth 0.8±0.1mm
2. Spall of 6±0.1 by 4±0.1 by 0.5±0.1mm
3. Surface crack of length – 15mm, thickness – 0.36±0.1mm depth – 2.1±0.1mm

The combined fault has 0.32% volume of pitting, 0.32% of spalling and 0.32% surface crack resulting in

1. 3 pits – 0.7±0.1 radius, 0.8±0.1 depth
2. Spall – 4±0.1 by 2±0.1 by 0.5±0.1mm
3. Surface crack depth of 0.7±0.1mm

Figure 6 clearly shows the healthy TVMS curve and the regions of double and single engagement. In figure 7, the curve denoted by km is the healthy mesh stiffness to be used as a reference. The second curve kms is for the spalling fault and a relatively huge reduction in the mesh stiffness is seen in the region of the fault. The curve kmp represents pitting and the reduction in TVMS is also seen. It is also clear that the TVMS reduces in line with the shape of the fault. This suggests that the shape of the faults affects the mesh stiffness obtained. The next curve, which is kmc also brings about a reduction in stiffness based on the crack affected area. The TVMS curve of the combined fault denoted by kmm shows a shows major reduction in TVMS in the regions of combined faults and this region has the lowest TVMS of 5.8 x10^8 N/m

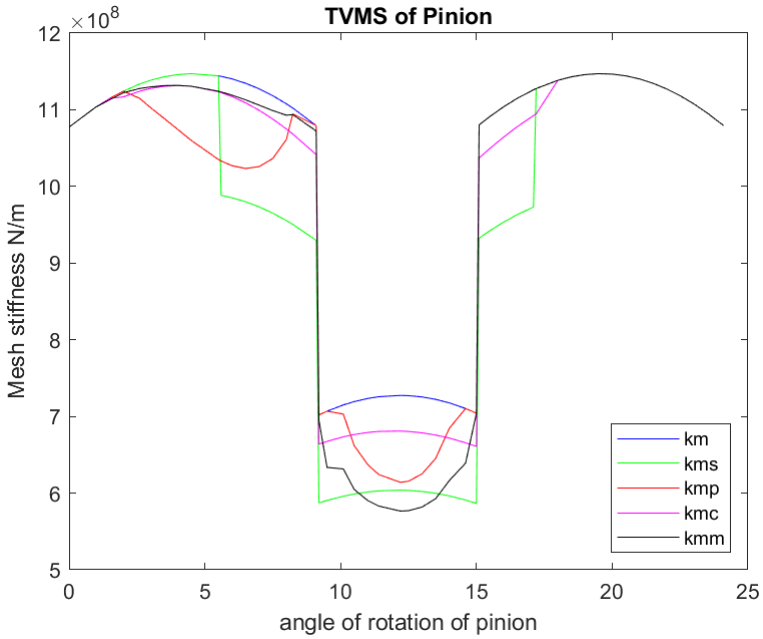

Figure 7: TVMS plot of Gear pair with damage pinion -pit (kmp), spall (kms), surface crack (kmc), multiple (kmm)

Conclusion

In this work, a method was proposed for the evaluation of the TVMS of multiple faults on a gear tooth. The potential energy method was used to analytically determine the stiffnesses. The results from the TVMS of the multiple faults of 0.96% of the tooth volume – 0.32% pits, 0.32% spall, and 0.32% surface crack were compared with the same volume of faults for each single fault that comprised the multiple faults namely 0.96% single pitting, 0.96% single spall volume and 0.96% single surface crack tooth volume. All fault conditions resulted in a decrease in TVMS, and the shape of the decrease was influenced by the shape of the fault. It is noted that the combination of faults results in a relatively higher drop in the mesh stiffness than the single faults as the section with the fault combination represents the lowest dip in all the TVMS curves. This suggests that accurate

representation of gear tooth faults in service is required to accurately evaluate the mesh stiffness and hence dynamic response of damaged gears.

References

[1] Z. Meng, G. Shi, F. Wang, Vibration response and fault characteristics analysis of gear based on time-varying mesh stiffness, Mech Mach Theory 148 (2020) 103786. https://doi.org/10.1016/J.MECHMACHTHEORY.2020.103786.

[2] J.D.M. Marafona, P.M.T. Marques, R.C. Martins, J.H.O. Seabra, Mesh stiffness models for cylindrical gears: A detailed review, Mech Mach Theory 166 (2021) 104472. https://doi.org/10.1016/J.MECHMACHTHEORY.2021.104472.

[3] A. Oreavbiere, M. Khan, Mathematical Complexities in Modelling Damage in Spur Gears, Machines 12 (2024). https://doi.org/10.3390/machines12050346.

[4] D.C. H Yang Assistant Professor Assoc Mem ASME J Y Lin, Hertzian Damping, Tooth Friction and Bending Elasticity in Gear Impact Dynamics, 1987. http://asmedigitalcollection.asme.org/mechanicaldesign/article-pdf/109/2/189/5560695/189_1.pdf.

[5] Xinhao. Tian, Dynamic simulation for system response of gearbox including localized gear faults, Library and Archives Canada = Bibliothèque et Archives Canada, 2005.

[6] X. Liang, M.J. Zuo, Z. Feng, L. Liu, A mesh stiffness evaluation model to reflect tooth pitting growth of a pair of external spur gears, in: Proceedings of 2016 Prognostics and System Health Management Conference, PHM-Chengdu 2016, Institute of Electrical and Electronics Engineers Inc., 2017. https://doi.org/10.1109/PHM.2016.7819811.

[7] X. Liang, H. Zhang, L. Liu, M.J. Zuo, The influence of tooth pitting on the mesh stiffness of a pair of external spur gears, Mech Mach Theory 106 (2016) 1–15. https://doi.org/10.1016/J.MECHMACHTHEORY.2016.08.005.

[8] W. Liu, R. Zhu, W. Zhou, Y. Shang, Probability distribution model of gear time-varying mesh stiffness with random pitting of tooth surface, Eng Fail Anal 130 (2021). https://doi.org/10.1016/j.engfailanal.2021.105782.

[9] T. Chen, Y. Wang, Z. Chen, A novel distribution model of multiple teeth pits for evaluating time-varying mesh stiffness of external spur gears, Mech Syst Signal Process 129 (2019) 479–501. https://doi.org/10.1016/J.YMSSP.2019.04.029.

[10] J. Hou, S. Yang, Q. Li, Y. Liu, Effect of a Novel Tooth Pitting Model on Mesh Stiffness and Vibration Response of Spur Gears, Mathematics 10 (2022). https://doi.org/10.3390/math10030471.

[11] T. Chen, Y. Wang, Z. Chen, A novel distribution model of multiple teeth pits for evaluating time-varying mesh stiffness of external spur gears, Mech Syst Signal Process 129 (2019) 479–501. https://doi.org/10.1016/J.YMSSP.2019.04.029.

[12] Y. Lei, Z. Liu, D. Wang, X. Yang, H. Liu, J. Lin, A probability distribution model of tooth pits for evaluating time-varying mesh stiffness of pitting gears, Mech Syst Signal Process 106 (2018) 355–366. https://doi.org/10.1016/J.YMSSP.2018.01.005.

[13] X.H. Liang, Z.L. Liu, J. Pan, M.J. Zuo, Spur Gear Tooth Pitting Propagation Assessment Using Model-based Analysis, Chinese Journal of Mechanical Engineering (English Edition) 30 (2017) 1369–1382. https://doi.org/10.1007/s10033-017-0196-z.

[14] J. Liu, C. Wang, W. Wu, Research on Meshing Stiffness and Vibration Response of Pitting Fault Gears with Different Degrees, International Journal of Rotating Machinery 2020 (2020). https://doi.org/10.1155/2020/4176430.

[15] Z. Meng, F. Wang, G. Shi, A novel evolution model of pitting failure and effect on time - varying meshing stiffness of spur gears, Eng Fail Anal 120 (2021) 105068. https://doi.org/10.1016/J.ENGFAILANAL.2020.105068.

[16] Yunxia Chen, Yi Jin, Rui Kang, Wenjun Gong, Yi Yang, The Time-varying Mesh Stiffness Modeling of Gear System with Spalling Defects in Different Positions, in: 2017 4th International Conference on Transportation Information and Safety (ICTIS) : Conference Proceedings : Banff, Alberta, Canada, August 8-10, 2017: pp. 658–663.

[17] F. Wang, P. Dai, S. Yan, J. Wang, L. Niu, Investigation on double shock in vibration response of the gear pair with spalling defects, Proc Inst Mech Eng C J Mech Eng Sci 237 (2023) 4882–4894. https://doi.org/10.1177/09544062231153743.

[18] Y. Luo, N. Baddour, M. Liang, Evaluation of time-varying mesh stiffness of gears with tooth spalls modeled as spherical shapes, in: Proceedings - 2018 Prognostics and System Health Management Conference, PHM-Chongqing 2018, Institute of Electrical and Electronics Engineers Inc., 2019: pp. 94–99. https://doi.org/10.1109/PHM-Chongqing.2018.00022.

[19] S. Wang, R. Zhu, An improved mesh stiffness calculation model of spur gear pair under mixed EHL friction with spalling effect, in: Vibroengineering Procedia, EXTRICA, 2020: pp. 176–181. https://doi.org/10.21595/vp.2020.21671.

[20] Y. Huangfu, K. Chen, H. Ma, X. Li, H. Han, Z. Zhao, Meshing and dynamic characteristics analysis of spalled gear systems: A theoretical and experimental study, Mech Syst Signal Process 139 (2020). https://doi.org/10.1016/j.ymssp.2020.106640.

[21] L. Shi, J. Wen, B. Pan, Y. Xiang, Q. Zhang, C. Lin, Dynamic characteristics of a gear system with double-teeth spalling fault and its fault feature analysis, Applied Sciences (Switzerland) 10 (2020) 1–23. https://doi.org/10.3390/app10207058.

[22] W. Luo, B. Qiao, Z. Shen, Z. Yang, H. Cao, X. Chen, Investigation on the influence of spalling defects on the dynamic performance of planetary gear sets with sliding friction, Tribol Int 154 (2021). https://doi.org/10.1016/j.triboint.2020.106639.

[23] L. Xiang, C. An, Y. Zhang, A. Hu, Failure dynamic modelling and analysis of planetary gearbox considering gear tooth spalling, Eng Fail Anal 125 (2021). https://doi.org/10.1016/j.engfailanal.2021.105444.

[24] W. Luo, B. Qiao, Z. Shen, Z. Yang, X. Chen, Time-varying mesh stiffness calculation of a planetary gear set with the spalling defect under sliding friction, Meccanica 55 (2020) 245–260. https://doi.org/10.1007/s11012-019-01115-y.

[25] W. Yu, C.K. Mechefske, M. Timusk, A new dynamic model of a cylindrical gear pair with localized spalling defects, Nonlinear Dyn 91 (2018) 2077–2095. https://doi.org/10.1007/s11071-017-4003-2.

[26] Y. Luo, N. Baddour, G. Han, F. Jiang, M. Liang, Evaluation of the time-varying mesh stiffness for gears with tooth spalls with curved-bottom features, Eng Fail Anal 92 (2018) 430–442. https://doi.org/10.1016/j.engfailanal.2018.06.010.

[27] A. Saxena, A. Parey, M. Chouksey, Time varying mesh stiffness calculation of spur gear pair considering sliding friction and spalling defects, Eng Fail Anal 70 (2016) 200–211. https://doi.org/10.1016/J.ENGFAILANAL.2016.09.003.

[28] L. Zhang, Y. Shao, Mesh Stiffness Calculation of Spur Gears with Tooth Surface Crack, in: Proceedings of the ASME 2019 International Design Engineering Technical Conferences and Computers and Information in Engineering Conference IDETC/CIE2019 August 18-21, 2019, Anaheim, CA, USA, 2019. http://asmedigitalcollection.asme.org/IDETC-CIE/proceedings-pdf/IDETC-CIE2019/59308/V010T11A011/6454683/v010t11a011-detc2019-97857.pdf.

[29] F. Chaari, W. Baccar, M.S. Abbes, M. Haddar, Effect of spalling or tooth breakage on gearmesh stiffness and dynamic response of a one-stage spur gear transmission, European Journal of Mechanics, A/Solids 27 (2008) 691–705. https://doi.org/10.1016/j.euromechsol.2007.11.005.

[30] F. Chaari, T. Fakhfakh, M. Haddar, Analytical modelling of spur gear tooth crack and influence on gearmesh stiffness, European Journal of Mechanics - A/Solids 28 (2009) 461–468. https://doi.org/10.1016/J.EUROMECHSOL.2008.07.007.

[31] O.D. Mohammed, M. Rantatalo, Dynamic response and time-frequency analysis for gear tooth crack detection, Mech Syst Signal Process 66–67 (2016) 612–624. https://doi.org/10.1016/J.YMSSP.2015.05.015.

[32] O.D. Mohammed, M. Rantatalo, Gear tooth crack detection using dynamic response analysis, Insight: Non-Destructive Testing and Condition Monitoring 55 (2013) 417 – 421. https://doi.org/10.1784/insi.2012.55.8.417.

[33] M. Onkareshwar, V. Inturi, S.P. Rajendra, P.K. Penumakala, G.R. Sabareesh, Effect of local gear tooth failures on gear mesh stiffness and vibration response of a single-stage spur gear pair, in: Lecture Notes in Mechanical Engineering, Springer Science and Business Media Deutschland GmbH, 2021: pp. 1095–1103. https://doi.org/10.1007/978-981-15-8049-9_69.

[34] J. Ning, Z. Chen, Y. Wang, Y. Li, W. Zhai, Vibration feature of spur gear transmission with non-uniform depth distribution of tooth root crack along tooth width, Eng Fail Anal 129 (2021). https://doi.org/10.1016/j.engfailanal.2021.105713.

[35] Z. Chen, W. Zhai, Y. Shao, K. Wang, G. Sun, Analytical model for mesh stiffness calculation of spur gear pair with non-uniformly distributed tooth root crack, Eng Fail Anal 66 (2016) 502–514. https://doi.org/10.1016/J.ENGFAILANAL.2016.05.006.

[36] Z. Chen, Y. Shao, Dynamic simulation of spur gear with tooth root crack propagating along tooth width and crack depth, Eng Fail Anal 18 (2011) 2149–2164. https://doi.org/10.1016/J.ENGFAILANAL.2011.07.006.

[37] O.D. Mohammed, M. Rantatalo, J.O. Aidanpää, Dynamic modelling of a one-stage spur gear system and vibration-based tooth crack detection analysis, Mech Syst Signal Process 54–55 (2015) 293–305. https://doi.org/10.1016/J.YMSSP.2014.09.001.

[38] L.T. Yang, Y.M. Shao, W.W. Jiang, L.K. Zhang, L.M. Wang, J. Xu, Effects of tooth surface crack propagation on meshing stiffness and vibration characteristic of spur gear system, Applied Sciences (Switzerland) 11 (2021) 1–18. https://doi.org/10.3390/app11041968.

[39] W. Chen, Y. Lei, Y. Fu, L. Hou, A study of effects of tooth surface wear on time-varying mesh stiffness of external spur gear considering wear evolution process, Mech Mach Theory 155 (2021). https://doi.org/10.1016/j.mechmachtheory.2020.104055.

[40] Z. Shen, L. Yang, B. Qiao, W. Luo, X. Chen, R. Yan, Mesh relationship modeling and dynamic characteristic analysis of external spur gears with gear wear, Frontiers of Mechanical Engineering 17 (2022). https://doi.org/10.1007/s11465-021-0665-z.

[41] Y. Wang, K. Li, B. Qiao, Z. Shen, X. Chen, Theoretical Investigation of Mesh Relationship and Mesh Stiffness of Internal Spur Gears with Tooth Wear, Applied Sciences (Switzerland) 13 (2023). https://doi.org/10.3390/app13032022.

[42] N. Dong, Q. Cui, J. Zhou, R. Tong, H. Wang, F. Lu, Study on wear evolution of spur gears considering dynamic meshing stiffness, Journal of Mechanical Science and Technology 37 (2023) 3393–3408. https://doi.org/10.1007/s12206-023-0606-3.

[43] T. Ouyang, G. Wang, L. Cheng, J. Wang, R. Yang, Comprehensive diagnosis and analysis of spur gears with pitting-crack coupling faults, Mech Mach Theory 176 (2022). https://doi.org/10.1016/j.mechmachtheory.2022.104968.

[44] O. Asi, Fatigue failure of a helical gear in a gearbox, Eng Fail Anal 13 (2006) 1116–1125. https://doi.org/10.1016/J.ENGFAILANAL.2005.07.020.

[45] A. Parey, N.K. Jain, S.C. Koria, Failure analysis of air cooled condenser gearbox, Case Stud Eng Fail Anal 2 (2014) 150–156. https://doi.org/10.1016/J.CSEFA.2014.08.003.

[46] V. Rajinikanth, M.K. Soni, B. Mahato, M.A. Rao, Microstructural investigation of rolling contact fatigue (RCF) on a failed planetary gear of a windmill gearbox, Eng Fail Anal 121 (2021). https://doi.org/10.1016/j.engfailanal.2020.105167.

[47] Q. Wang, Y. Zhu, Z. Zhang, C. Fu, C. Dong, H. Su, Partial Load: A Key Factor Resulting in the Failure of Gear in the Wind Turbine Gearbox, Journal of Failure Analysis and Prevention 16 (2016) 109–122. https://doi.org/10.1007/s11668-015-0057-y.

https://dspace.org/

Comparison of the time varying mesh stiffness of gears with single and multi-mode damage

Oreavbiere, Aselimhe; Khan, Muhammad

2025-11-01
Trans Tech Publications
https://doi.org/10.4028/p-ebn8qs
Oreavbiere A, Khan M. (2025) Comparison of the time varying mesh stiffness of gears with single and multi-mode damage. Key Engineering Materials, Volume 1033, November 2025, pp. 59-70

Downloaded from a DSpace repository. https://dspace.org/